J Mater Sci (2007) 42:5196–5202
DOI 10.1007/s10853-006-0458-0

Carbon dioxide reduction into carbon by mechanically milled wustite

Eiji Yamasue · Hironori Yamaguchi · Hiroshi Nakaoku · Hideyuki Okumura · Keiichi N. Ishihara

Received: 7 March 2006 / Accepted: 16 May 2006 / Published online: 23 February 2007

Abstract The CO_2 decomposition utilizing mechanically milled wustite powders was qualitatively and quantitatively examined and its mechanism was investigated. The wustite phase is stable at least up to 6 h of milling, and the lattice parameter, the crystallite size and the average particle diameter are monotonously decreased with milling time, while the BET specific surface area is correspondingly increased. The mechanically milled FeO powder decomposes CO_2 into graphite and amorphous carbon at 773 K, where the decomposition intensity increases with milling time, while unmilled FeO decomposes CO_2 into CO with the same annealing condition. It is found that the FeO powder thermally decomposes into Fe and Fe_3O_4 prior to the reaction with CO_2, followed by the precipitated Fe reacting with CO_2, and also that the thermal decomposition is promoted by the milling process.

E. Yamasue (✉) · H. Okumura · K. N. Ishihara
Graduate School of Energy Science, Kyoto University,
Yoshida-Honmachi Sakyo-ku, Kyoto 606-8501, Japan
e-mail: yamasue@energy.kyoto-u.ac.jp

H. Yamaguchi
Graduate School of Science, Kyoto University,
Yoshida-Honmachi Sakyo-ku, Kyoto 606-8501, Japan

H. Nakaoku
Institute of Industrial Science, University of Tokyo, 4-6-1,
Komaba Meguro-ku, Tokyo 153-8505, Japan

Introduction

Carbon dioxide is one of the greenhouse gases, and the development of materials that can fix carbon dioxide is required for our sustainable society. The direct decomposition of carbon dioxide into carbon using iron oxides has been actively studied in recent years. Tamaura et al. [1] reported the reduction of carbon dioxide into carbon with an efficiency of nearly 100% at 563 K using ''active magnetite'', i.e. iron-excess magnetite ($Fe_{3.127}O_4$ or $Fe_3O_{3.838}$). Zhang et al. [2–4] reported the same reaction even at room temperature using another oxygen-deficient active magnetite, ($Fe_3O_{3.8676}$). These active magnetites, which are produced by keeping ordinary magnetite in an H_2 atmosphere, are stable in an Ar gas, but unstable in air at room temperature i.e. to return to the ordinary magnetite by oxidation. On the other hand, Kodama et al. [5] and Zhang et al. [6] reported that ''active wustite'' ($Fe_{0.98}O$) reacts with CO_2 to produce C and magnetite.

It is not only technologically important but also scientifically interesting to activate iron oxides in terms of the reactivity with CO_2. Mechanical milling is one of the most popular and effective methods to produce non-equilibrium state with a large number of defects and even a change in the crystal structure. It was originally developed in 1970 [7] to achieve a particle dispersion strengthening superalloy, and in recent years, much attention is paid as one of the methods to produce non-equilibrium materials [8, 9]. During the mechanical milling process, the repeated addition of mechanical power can urge to grind powders to alloy them through a solid state reaction, and/or to produce the non-equilibrium state such as supersaturated solid

solution, metastable phase, nanocrystal and amorphous. Thus, such active magnetites and active wustite mentioned above may also be formed by mechanical milling.

The aim of this study is to investigate the effect of mechanical milling on the state of the wustite and the ability of carbon dioxide fixation, proposing a new possible system resolving the global warming problem.

Experimental

The FeO powder of 99.9% purity (particle size –80 mesh) was used as the starting materials. Ten grams of the sample was measured in a glove box under an Ar atmosphere and put in a ball mill vial with 28 pieces of stainless steel balls (3.68 g a piece). The Ar gas was filled in the vial up to 0.2 MPa and no process control agent (PCA) was used. Mechanical milling (12 Hz) was performed for 1, 5, 10, 30, 60, 180 and 360 min using a high energy vibration ball milling machine (Supermisuni NEV-MA8, Nissin-Giken Co. Ltd., Saitama Japan). The milled powder was sampled in an Ar atmosphere.

The schematic diagram of the experimental apparatus for CO_2 decomposition is shown in Fig. 1. Five grams of the milled sample (corresponding to 7.0×10^{-2} mol of stoichiometric FeO) on an alumina boat was placed in a quartz tube (the inner volume is 5.71×10^{-4} m^3) with CO_2 at 0.05 MPa, and the tube was heat treated in a furnace at 773 K for 180 min. The inner pressure change was monitored every 5 min.

The carbon content in the powder after CO_2 decomposition was measured using the Carbon/Sulfur Determinator (CS-444, LECO Co. Ltd.). Powder X-ray diffractometry (XRD) with Cu-Kα radiation was performed utilizing RINT2000 (Rigaku Co. Ltd., Japan). The morphology of the powder was observed using scanning electron microscopy, SEM (JSM-5800 TYPE-C, JEOL Ltd., Tokyo Japan). The single-point BET specific surface area measurements were performed using a flow gas method (Flowsorb III 2300, Micromeritics), where the carrier gas with a mixture of 30% N_2 and 70% He was used.

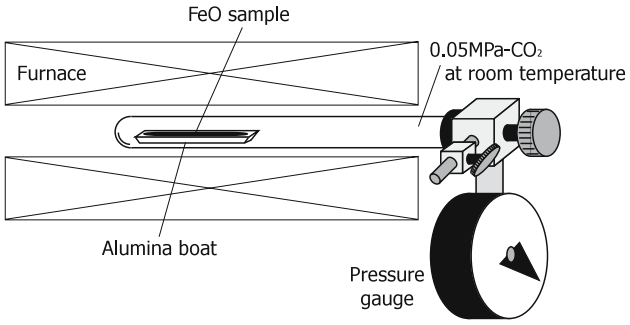

Fig. 1 Schematic diagram of the experimental apparatus for CO_2 decomposition experiment

Results

SEM images of the FeO powders for (a) prior to the milling process, and after the milling for (b) 5, (c) 10, (d) 30 and (e) 360 min are shown in Fig. 2. The particle size is rapidly decreased with milling for short periods of time (i.e. less than 10 min), but the decrease rate becomes sluggish after 30 min of milling. The average particle diameters were then estimated from the SEM images using an image analysis software, based on an assumption that the particles are spherical and shown in Fig. 3. The particle size rapidly decreases at an early stage of milling process and shows an almost constant value after 60 min of milling. The BET surface areas of the powder samples monotonously increase with milling time as shown in Fig. 3, and they exhibit a linear relationship with the inverses of the average particle diameter.

The X-ray diffraction patterns of the FeO powders are shown in Fig. 4. Before the milling process, all the X-ray peaks are identified as FeO with NaCl-type structure and Fe (Fig. 4a). As the milling time is increased (b–e), the positions of FeO peaks shift to the higher angle side, indicating decrease of the lattice parameter, while the Fe peak position does not change. The FeO peaks are broadened with milling time, indicating decrease of the crystallite size. The lattice parameters calculated from FeO(420) peak and the average crystallite size estimated by the Scherrer's formula from FeO(111) peak are summarized in Table 1 and Fig. 5. The crystallite size drastically decreases at an early stage of milling and shows almost constant value after 60 min, the tendency of which is similar to the particle size, while the lattice parameter is monotonously decreased with milling time. It is noted that, since the intensity ratio of the FeO peaks changes with milling time, the degree of order in the FeO lattice decreases with milling time. This may be the origin of the decrease in the lattice parameter.

Figure 6 shows the relation between the pressure decrease in the reaction tube and the reaction time at 773 K for the FeO powders milled for 0, 1, 5, 10, 30, 60, 180 and 360 min, where the pressure change of the reaction tube without sample was used as a standard.

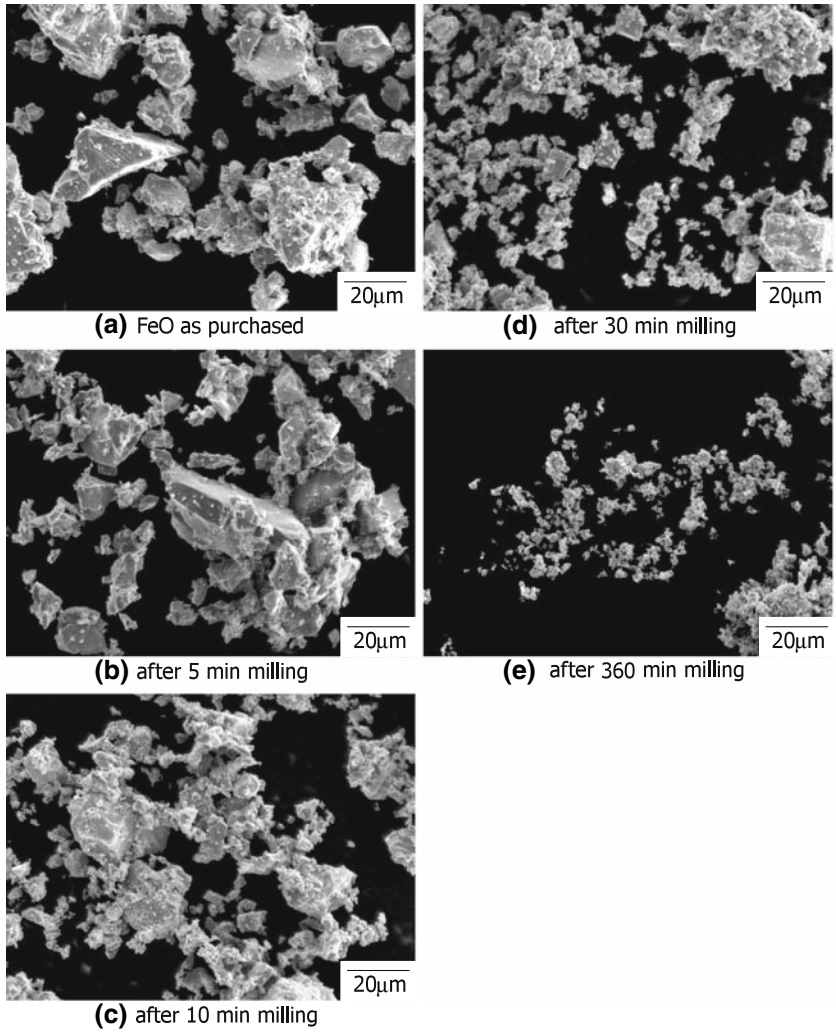

Fig. 2 SEM images of (a) FeO powder prior to milling process, after (b) 5 min, (c) 10 min, (d) 30 min (e) 360 min milling

No pressure decrease can be observed for the samples of 0 and 1-min-milling but each weight is increased by 0.082 g after 180 min of the reaction, indicating the oxidation of FeO with CO_2. On the other hand, as for the longer-milled samples, the pressure, indicating decomposition of carbon dioxide, is rapidly decreased and followed by near-plateau. The pressure of each near-plateau region decreases with milling time up to 30 min, but no further change for longer milling times. From here on, the FeO samples milled for 0 (without milling) and 1 min are classified as Group A, and the other samples milled for longer times as Group B, respectively.

X-ray diffraction patterns of the FeO powders without milling (representing group A) and milled for 360 min (representing group B) after the CO_2 decomposition are shown in Fig. 7. For both A and B, Fe_3O_4 is produced as a major phase after the reaction, indicating that FeO is oxidized with CO_2. Small Bragg reflections of FeO and Fe are also observed for the group A, while only Fe_3O_4 phase is identified for B.

Figure 8 shows the carbon contents in the milled powder after the CO_2 decomposition experiments (•; measured by LECO) and in the consumed CO_2 (□; estimated from the pressure drop) plotted as a function of milling time, as well as the weight increase of the samples. The carbon content measurements by LECO were carried out at least five times and good reproducibility was obtained. No trace of carbon is detected for samples of group A, despite the weight increase of 0.082 g.

Thus, it is summarized for the samples of group A that, after the reaction with CO_2, (i) the inner pressure of the tube does not change during the reaction, (ii) Fe_3O_4 phase is produced and (iii) the sample weight is increased by 0.082 g (1.6 mass%) but (iv) no carbon is detected. From these facts, a following overall reaction is deduced;

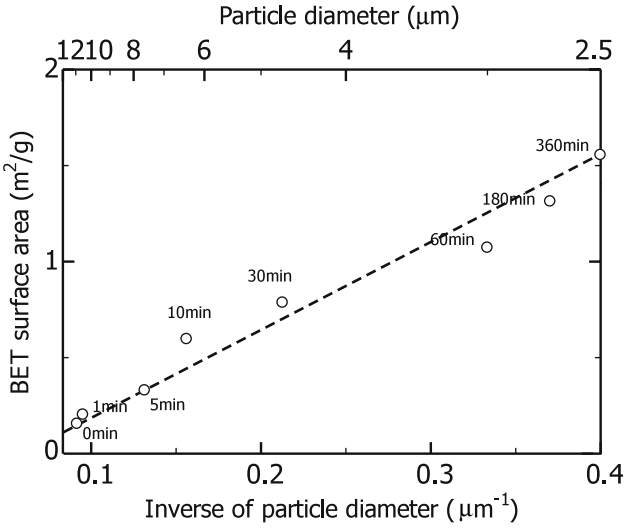

Fig. 3 Relation between the BET specific surface area and the inverse of particle size

$$3FeO(s) + CO_2(g) \rightarrow Fe_3O_4(s) + CO(g), \quad (I)$$

assuming the stoichiometric expression of FeO. The increase in weight is thus ascribed to the difference in Fe/O ratio between FeO and Fe_3O_4. The molar quantity of oxygen atom newly combined with FeO may be calculated as 5.1×10^{-3} mol, assuming that only oxygen atom contributes to the weight increase. Then, 1.5×10^{-2} mol of FeO with a stoichiometric composition, which is 22% of the initial amount of FeO, is consumed during the reaction. Since a majority of the FeO phase disappears after the CO_2 decomposition experiment (Fig. 7), a large quantity of FeO (about 78% of the initial amount of FeO), which does not contribute to the CO_2 decomposition, thermally decomposes into Fe and Fe_3O_4 by a eutectoid reaction [10–12].

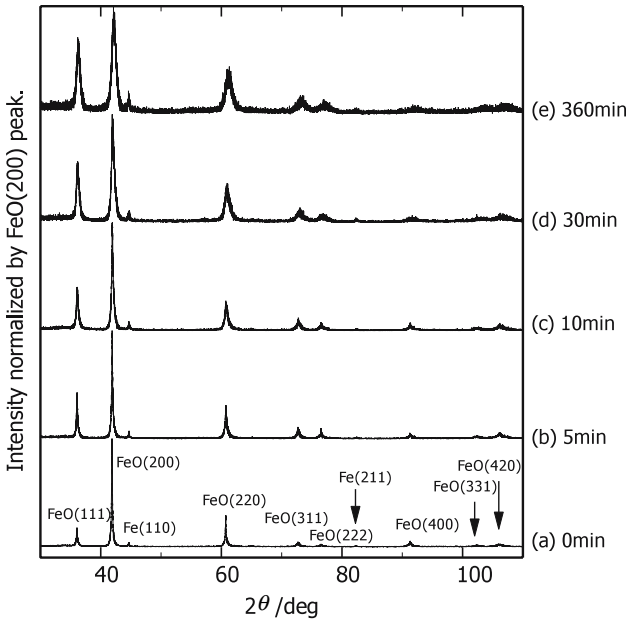

Fig. 4 X-ray diffraction patterns of (a) FeO powder prior to milling process, after (b) 5 min, (c) 10 min, (d) 30 min, (e) 360 min milling

Table 1 Average particle diameter, BET specific surface area, lattice parameter and crystallite size of FeO powder prior to milling process, after 1, 5, 10, 30, 60, 180 and 360 min milling

Period of milling time (min)	Average particle diameter (SEM)(μm)	Specific BET surface area (m^2/g)	Lattice parameter (nm)	Crystallitesize (nm)
0	10.9	0.155	0.4311	360
1	10.5	0.203	0.4310	340
5	7.6	0.329	0.4309	300
10	6.4	0.596	0.4308	220
30	4.7	0.786	0.4306	150
60	3.0	1.072	0.4300	120
180	2.7	1.313	0.4284	93
360	2.5	1.555	0.4276	86

As for the samples of group B, on the other hand, (i) the inner pressure is largely decreased during the reaction, (ii) Fe_3O_4 phase is produced, (iii) the sample weight is increased, and (iv) carbon is detected after the reaction (Fig. 8). Here, in order to identify the carbon-containing phases; graphite, amorphous or cementite, the powder sample after the reaction was dissolved in a concentrated hydrochloric acid (HCl) solution, and the X-ray diffractometry was performed on the residue. As shown in Fig. 9, it is comprised of graphite and amorphous carbon. The following reaction therefore takes place for the samples (majority) of group B;

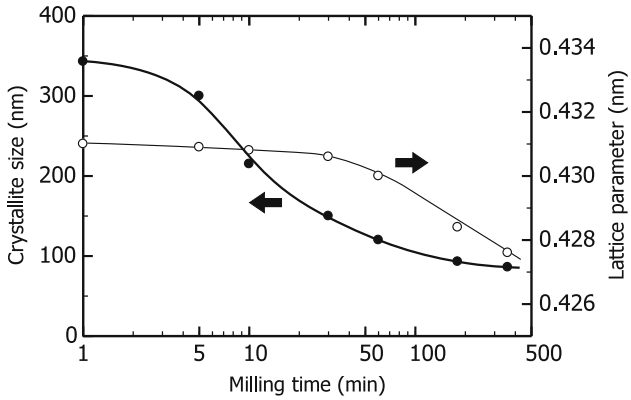

Fig. 5 Changes of crystallite size and lattice parameter as a function of milling time

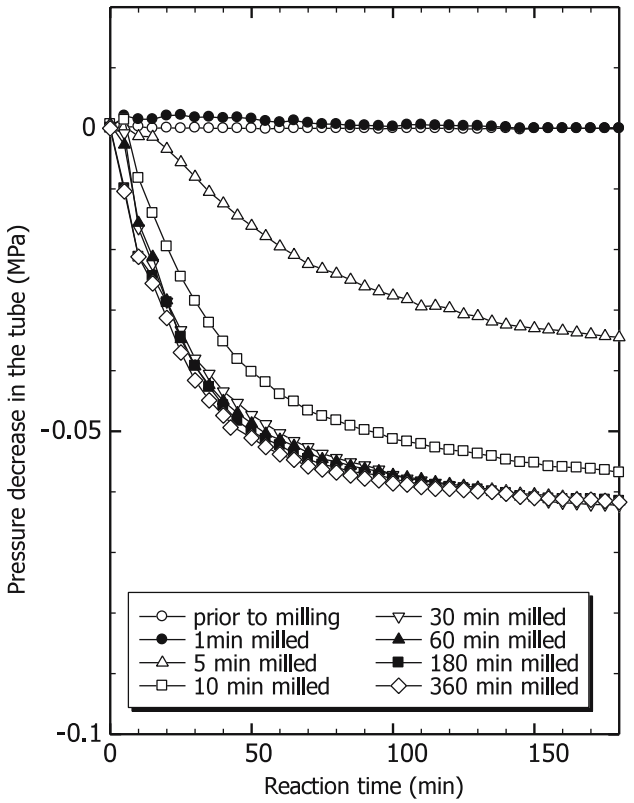

Fig. 6 The relation between inner pressure of the reaction tube and reaction time at 773 K for the FeO powder prior to milling process, FeO powder after 1, 5, 10, 30, 60, 180 and 360 min milling

$$6FeO(s) + CO_2(g) \rightarrow 2Fe_3O_4(s) + C(s). \quad (II)$$

The increase in weight is thus ascribed to the fixation of both oxygen (as Fe_3O_4) and carbon, which

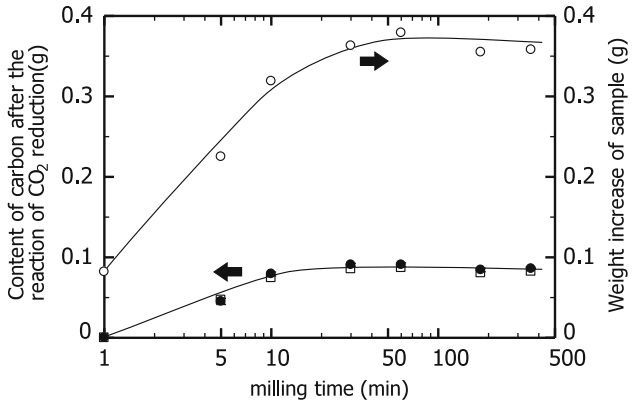

Fig. 8 The carbon contents (• measured by LECO and □ estimated from pressure change in the tube) and weight increases of the samples after CO_2 decomposition at 773 K for 3 h

is supported by the agreement of carbon contents determined from two different methods as also shown in Fig. 8. The reacted molar quantities of CO_2 as a function of milling time are shown in Fig. 10, which are estimated from the measured carbon content and the total weight increase, by assuming that (i) the amount of initially contained Fe in FeO is ignored, (ii) non-stoichiometric composition of FeO is ignored and (iii) both reactions (I) and (II) are the only reactions that proceed during the experiment.

The possible small amount of Fe_3C may be originated from the iron that was initially contained in the FeO powders since, when the same experiment is performed using elemental iron powder with diameters of 20–60 μm, only Fe_3C is detected after the reaction. Various carbon-containing phases, the carbon of which is derived from the CO_2 gas phase, are summarized in

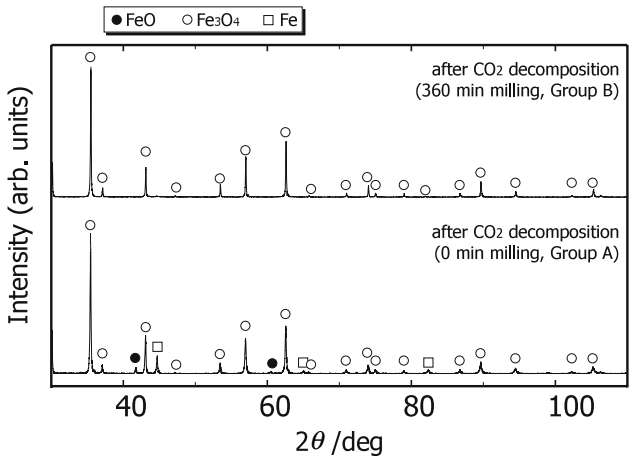

Fig. 7 X-ray diffraction patterns of the FeO powders after CO_2 decomposition at 773 K for 0 min and 360 min milled samples

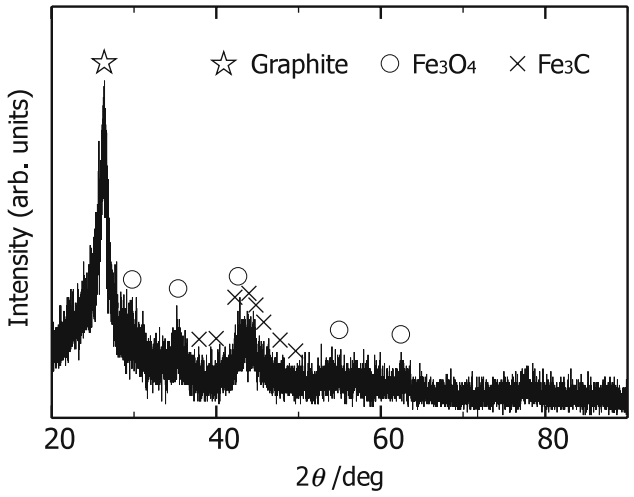

Fig. 9 X-ray diffraction pattern of the undissolved substance after HCl washing of the sample after CO_2 decomposition

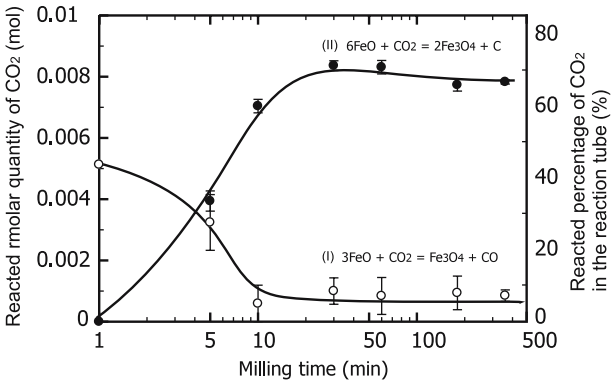

Fig. 10 The reacted molar quantities of CO_2 estimated for the reaction (I) $3FeO + CO_2 = Fe_3O_4 + CO$ (open circle) and (II) $6FeO + CO_2 = 2Fe_3O_4 + C$ (solid circle) as a function of milling time, both after 180 min of the CO_2 decomposition experiment at 773 K

Table 2, depending on the powder kind and the heating conditions.

Discussion

According to the Fe–O phase diagram [12], FeO thermally decomposes into Fe and Fe_3O_4 below 843 K, and the reaction may happen prior to the CO_2 decomposition event. Thus, the following three scenarios may be considered to explain the difference in CO_2 decomposition behavior between the samples of group A and B;

(i) FeO directly reacts with CO_2, followed by the thermal decomposition of the remained FeO.
(ii) The FeO of group B first decomposes into Fe and Fe_3O_4 through the eutectoid reaction and the produced Fe decomposes CO_2 into C, while FeO of group A directly decomposes CO_2 into CO prior to the thermal decomposition.
(iii) All the FeO samples first decompose into Fe and Fe_3O_4, followed by the reaction of the produced Fe decomposing CO_2 into C for group B (or CO for group A).

Table 2 Various carbon containing-phases derived from CO_2, depending on the powder kinds and heating conditions

Powder kind and heating conditions	Carbon-containing phase derived from CO_2
Elemental iron (20–60 μm), 773 K	Fe_3C
Active wustite (≈0.5 μm), 573 K [5, 6]	Amorphous carbon (90%) + Fe_3C (10%)
Unmilled FeO (Group A) (≈10 μm), 773 K	CO gas
Milled FeO (Group B) (<7.6 μm), 773 K	Graphite, amorphous carbon and trace of Fe_3C

When the unmilled FeO sample (representing group A) and the 60-min-milled sample (representing group B) are exposed to Ar instead of CO_2 at 773 K, the latter sample mostly decomposes into Fe and Fe_3O_4 after 10 min of heating, while the former sample still contains FeO even after 180 min (Fig. 11a, b, d and e). Thus, the milled FeO decomposes into Fe and Fe_3O_4 faster than unmilled FeO. When the heat-treated samples of (b) and (e) are further exposed to CO_2 at 773 K, similar changes in the phase (Fig. 11c, f), tube pressure and carbon contents to the previous experiments are observed (the unmilled FeO sample decomposes CO_2 into CO and the 60-min-milled sample decomposes CO_2 into C). For both samples, the X-ray peaks of Fe decrease, while those of Fe_3O_4 increase (Fig. 11d, g), indicating the Fe reacting with CO_2. This suggests the decomposition of FeO into Fe and Fe_3O_4 prior to the reaction with CO_2 regardless of milling process, supporting the third scenario. Accordingly, the following reactions can be considered;

$$4FeO(s) \rightarrow Fe_3O_4(s) + Fe(s) \quad \text{(III)}$$

$$3Fe(s) + 4CO_2(g) \rightarrow Fe_3O_4(s) + 4CO(g) \quad \text{(Group A)} \quad \text{(IV)}$$

$$3Fe(s) + 2CO_2(g) \rightarrow Fe_3O_4(s) + 2C \quad \text{(Group B)} \quad \text{(V)}$$

Combinations of the reactions (III) and (IV) or (III) and (V) lead to the reactions (I) and (II), respectively.

When elemental iron is used for the same experiment, Fe_3C phase is produced as mentioned before. Thus, the trace of Fe_3C from our milled wustite may be ascribed to the elemental iron originally included in initial samples, as well as the reported small amount of Fe_3C from the active wustite [5, 6]. On the other hand, the thermally decomposed iron from our milled (or unmilled) wustite appears to decompose CO_2 into C (or CO), and furthermore, the active wustite is reported to decompose CO_2 into amorphous carbon [6]. Accordingly, it is suggested that the property of the thermally decomposed iron differs from the elemental iron, i.e., the former iron precipitates appear on the FeO powder with Fe_3O_4 phase, probably exhibiting complicated microstructure and defect structure (unlike pure bcc Fe particles). If the surface properties such as the strain state, the electronic charge state and/or the defect structure, are different from pure bcc Fe, it is not surprising to have the different

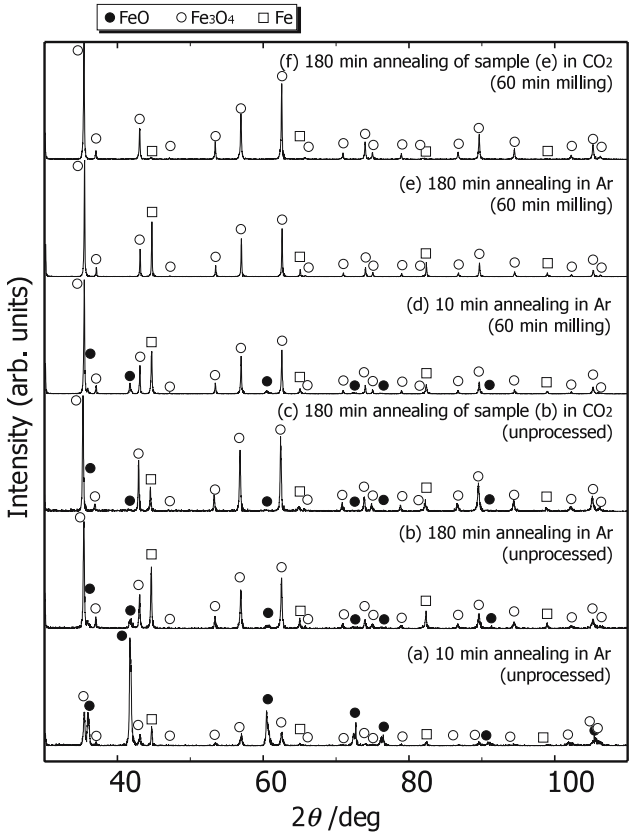

Fig. 11 X-ray diffraction patterns of unprocessed (a–c) and 60-min-milled (d–f) samples after various annealing conditions at 773 K. For (a), (b), (d) and (e), the annealing was performed in Ar atmosphere, while for (c) or (f) in CO_2 using sample (b) or (e), respectively

carbon-containing phase on it. It is also interesting to note that only the samples of group B decompose CO_2 into C. It is possible that the reduction of CO_2 may be a two-step process ($CO_2 \rightarrow CO \rightarrow C$) and there might be a critical threshold surface area of the precipitated Fe phase to achieve the carbon fixation. The variation of the reaction rate (II) coincides, in terms of the milling period, with the variation in the surface area, the particle diameter and the crystallite size (Fig. 10), rather than the lattice parameter. This supports that the thermal decomposition prior to the reaction with CO_2, which should provide a large surface area of the precipitated Fe, controls the reaction (II) since the size-scale of a material is often maintained after a thermal decomposition. The details of the mechanism are still not clear, and further investigation is necessary to attain the effective carbon fixation system.

Conclusion

The CO_2 decomposition utilizing mechanically milled FeO powders was qualitatively and quantitatively examined and its mechanism was investigated. The wustite phase is stable at least up to 6 h of milling, and the lattice parameter, the crystallite size and the average particle diameter are monotonously decreased with milling time. The corresponding specific surface area of the FeO powder is increased with milling time, and exhibits a linear relation with the reciprocal of the particle diameter.

The mechanically milled FeO powder decomposes CO_2 into graphite and amorphous carbon at 773 K, where the decomposition intensity increases with milling time, while unmilled FeO decomposes CO_2 into CO, and elemental iron decomposes CO_2 into Fe_3C. The FeO powder thermally decomposes into Fe and Fe_3O_4 prior to the reaction with CO_2, followed by the precipitated Fe reacting with CO_2 to produce various carbon-containing phases. The thermal decomposition is promoted by the milling process.

Acknowledgement This study was partially supported by New Energy and Industrial Technology Development Organization (NEDO), ''Industrial Technology Research Grant Program, 2001–2003'' and by Ministry of Education, Culture, Sports, Science and Technology, Grant-in-Aid for Young Scientists (B), 17760579, 2005.

References

1. Tamaura Y, Tabata M (1990) Nature 346:255
2. Zhang C, Li S, Wang L, Wu T, Peng S (2000) Mater Chem Phys 62:44
3. Zhang C, Li S, Wang L, Wu T, Peng S (2000) Mater Chem Phys 62:52
4. Zhang C, Wu T, Yang H, Jiang Y, Peng S (1996) Chinese Sci Bull 41(9):744
5. Kodama T, Tominaga K, Tabata M, Yoshida T, Tamaura Y (1992) J Am Ceram Soc 75(5):1287
6. Zhang C, Li S, Wu T, Peng S (1999) Mater Chem Phys 58:139
7. Benjamin JS (1970) Met Trans 1:2943
8. Murty BS, Ranganathan S (1998) Int Mater Rev 43:101
9. Suryanarayana C (2001) Progress Mater Sci 46:1
10. Darken LS, Gurry RW (1945) J Am Chem Soc 57:1398
11. Bransky I, Hed AZ (1968) J Am Chem Soc 51:231
12. Darken LS, Gurry RW (1946) J Am Chem Soc 68:798